Electron Transport Studies of Dye-Sensitized Solar Cells based on Natural Sensitizer Extracted from Rengas (*Gluta spp.*) and Mengkulang (*Heritiera elata*) Wood

Nur Ezyanie Safie,[a] Norasikin Ahmad Ludin,[a,*] Norul Hisham Hamid,[b,c]
Paridah Md. Tahir,[c] Mohd Asri Mat Teridi,[a] Suhaila Sepeai,[a] Mohd Adib Ibrahim,[a] and Kamaruzzaman Sopian [a]

Dyes extracted from rengas (*Gluta spp.*) and mengkulang (*Heritiera elata*) wood were investigated as sensitizers in dye-sensitized solar cells (DSSCs). Three types of sensitizers, including individual sensitizer, mixture sensitizer, and co-sensitizer, exhibited different patterns of absorption properties under UV-Vis spectroscopy. The incident photon-to-current efficiency (IPCE) was analyzed *via* spectral response to examine the generation of photocurrent. Because mixture sensitized DSSCs obtained broader absorption spectra, they were expected to achieve good light harvesting and hence, enhanced photocurrent and conversion efficiency. The photovoltaic performance was further examined by electrochemical impedance spectroscopy (EIS). The mixture sensitized DSSCs exhibited good conversion efficiency (0.21% and 0.30%) compared with individual sensitized DSSCs (0.16% and 0.11%). The co-sensitized DSSCs also showed increased conversion efficiency with ruthenium (N719) dye as a co-sensitizer. The parameters calculated from EIS analysis were used to determine suitable conditions for the dye to be implemented in DSSC. The behavior of electron transport was determined to be efficient due to the increase of electron diffusion coefficient, electron lifetime, and low recombination rate as achieved by the mixture sensitized DSSCs.

*Contact information: a: Solar Energy Research Institute (SERI), Universiti Kebangsaan Malaysia, 43600 Bangi, Selangor, Malaysia; b: Faculty of Forestry, Universiti Putra Malaysia, 43400 Serdang, Selangor, Malaysia; c: Institute of Tropical Forestry and Forest Products, Universiti Putra Malaysia, 43400 Serdang, Selangor, Malaysia: *Corresponding author: sheekeen@ukm.edu.my*

INTRODUCTION

The development of the dye-sensitized solar cell (DSSC) as an alternative device in solar energy applications has been extensively investigated. DSSCs have advantages such as lower cost and less toxic manufacture than conventional silicon-based cells (Shalini *et al.* 2015). Generally, DSSC devices are composed of a photoelectrode including the wide bandgap semiconductor metal oxide with adsorbed dye molecules and a counter-electrode made of a catalyst such as platinum covering the conducting glass. A mesoporous metal oxide such as TiO_2, ZnO, SnO_2, and Nb_2O_5 that is coated on the conducting glass is sintered to allow electronic conduction (Narayan 2012). Among them, anatase TiO_2, which has high dielectric constant, is the most common material used, as it provides good electrostatic shielding of the injected electron which then prevents from the recombination effects. The high refractive index of anatase TiO_2 also leads to an

efficient light scattering effect inside the porous photoelectrode, which is important to enhance light harvesting efficiency (Olea *et al.* 1999). The electrolyte is injected in between the electrodes to help in electron transport and in restoring reduced sensitizer. The most common electrolytes used are composed of the redox couples iodide/triiodide dissolved in liquid organic solvent (Faccio *et al.* 2011)

The principle of DSSC was proposed to mimic photosynthesis; the ability of the device to harvest visible light and convert chemical energy into electricity is very important (Koyama *et al.* 2009). Light is absorbed by a component known as the sensitizer, which is grafted on the TiO_2 surface of the photoelectrode. The role of the sensitizer is to supply electrons throughout the cell after being oxidized in the visible light range (380 nm to 800 nm). Generally, the sensitizer is made of metal-organic dyes, organic dyes, or natural derivative dyes.

The most stable and high conversion efficiency have been achieved with ruthenium (Ru) polypyridal compounds, such as *cis*-dithiocyanobis(4,4'-di-carboxy-2,2'-bipyridine) ruthenium(II) (N3), ditetrabutylammonium-*cis*-bis(isothiocyanato)bis(2,2'-bipyridyl-4,4'-dicarboxylatol)ruthenium(II) (N719), and tris-tetrabutylammonium tri-thiocyanato-4,4',4"-tricarboxy-2,2:6',2"-terpyridineruthenium(II) (black dye) (Nazeeruddin *et al.* 2001; Marwa *et al.* 2016; Wang *et al.* 2016). Although the conversion efficiency of ruthenium complex dyes is greater than 10%, there are some disadvantages that limit their potential. For instance, ruthenium is a rare, expensive metal that is not environmentally friendly (Adeloye and Ajibadebu 2014).

Organic dyes also are efficient sensitizers because of their satisfactory stability and large molar absorption coefficient (Zeng *et al.* 2014). Because organic dyes are metal-free, there is no concern about resource limitation, and their stereochemical structure can be modified (Ooyama and Harima 2012). The modification of molecular structures adjusts the absorption properties and rearranges the energy level of the sensitizer, resulting in better conversion efficiency. However, most molecular modifications of organic dyes require complicated synthesis procedures (Hara *et al.* 2005). Among the organic dyes, porphyrin-based DSSC has achieved a high conversion efficiency of 13% (Mathew *et al.* 2014).

Natural pigments are good alternative sensitizers because of the simple extraction procedure, low cost, and low environmental impact. These abundant natural pigments are present in some fruits, flowers, and leaves of plants; they contain compounds that strongly absorb visible light at different wavelengths, resulting in different visible colors (Lim *et al.* 2015). Several natural pigments have been extensively investigated, such as chlorophyll (Wang *et al.* 2010), anthocyanin (Ozuomba *et al.* 2013), xanthophyll (Kartini *et al.* 2015), and carotene (Shanmugam *et al.* 2013). While the conversion efficiencies achieved (< 3%) are much lower than the industrial requirements (Basheer *et al.* 2014), numerous studies have investigated various plant species as sources of sensitizers. This paper examines the performance of dye-sensitized solar cells based on natural sensitizers extracted from rengas (*Gluta* spp.) and mengkulang (*Heritiera elata*) wood. The highlight in this study is the electron transport mechanism inside the cells, which will predict any fault in the devices. The three types of sensitizers examined were an individual sensitizer (extracted from rengas (*Gluta* spp.) and mengkulang (*Heritiera elata*) wood), a mixture sensitizer (mixing both of the individual dyes), and a co-sensitizer (individual sensitizer co-sensitized with ruthenium (N719) dye). The electron kinetics of these sensitizers are discussed.

EXPERIMENTAL

Preparation of Sensitizers

The procedure for the synthesis of mengkulang and rengas dye has been detailed elsewhere (Safie *et al.* 2017). The crude extract from rengas and mengkulang was prepared by Soxhlet extraction. Methanol obtained from Sigma-Aldrich (St. Louis, MO, USA) was used as an organic solvent in the cold extraction of dye from the sawdust. The mixture was left overnight at room temperature before undergoing Soxhlet extraction and was handled in low light to minimize photooxidation. The crude extract was stored at 4 °C. Various dye solutions were prepared by mixing the individual dyes (mixture sensitizers) and co-sensitized mengkulang and rengas with ruthenium (N719) dye (co-sensitizers). To prepare a 0.3 mM N719 sensitizer, 50 mL acetonitrile (J. T. Baker® Chemicals, Philadelphia, PA, USA) and 50 mL 4 tert-butyl alcohol (99.7%, Sigma-Aldrich) were mixed with 0.036 g B2 (N719) dye (Dyesol, NSW, Queanbeyan, Australia). The mixture was incubated overnight at room temperature before use.

Assembly of the DSSCs

To prepare the photoelectrodes, fluorine-doped conducting tin oxide (FTO, ~15 Ω sq^{-1}, Solaronix SA, Aubonne, Switzerland) was cleaned and then washed sequentially with acetone and DI water in an ultrasonic cleaner. In this study, two layers of TiO_2 were used including porous and scattering layers as the first and second layer, respectively. TiO_2 paste (90 T, Dyesol) was coated onto the conducting surface of the FTO as the first layer by the doctor blading technique. The coated glass was heated at 450 °C for 30 min. The step was repeated followed by the second layer which is a TiO_2 paste (WER 2, Dyesol). The coated conducting glass was maintained with an active layer 1 cm^2 by scrapping the excess TiO_2. The TiO_2 thin film was immersed in various dye solutions at room temperature for 24 h to allow the dye molecules to adsorb to the TiO_2 surface. Before assembly, the TiO_2 thin film was rinsed using the organic solvent to remove excess dye that could lead to dye aggregation. The thin film was dried using nitrogen gas.

For the counter electrode, FTO glass (~8 Ω sq^{-1}, Solaronix) was coated with platinum paste (Solaronix) and sintered at 450 °C for 30 min. Both electrodes were separated by 60 µm-thick Surlyn® layer (Meltonix 1170-60, Solaronix) and sealed by heating. The redox electrolyte (iodolyte AN-50, Solaronix) was then injected to fill the gap between the electrodes. Polymer glue was applied around the edges of the cell to prevent the electrolyte from leaking after the injection.

Instrumentation and Measurement

The optical absorption properties of the dyes were obtained from a UV-Vis spectrophotometer (UV-1800, Shimadzu, Kyoto, Japan). Photoconversion properties of the cells were analyzed through the incident photo-to-current efficiency (IPCE) curve that was measured *via* spectral response measurement system (IVT Solar PVE-300, Bentham Instruments, Ltd., Berkshire, UK). The surface of the DSSC was exposed under an irradiation of 1000 W/m^2, and the photovoltaic performance was conducted using a class AAA solar simulator (XES-40S1, San-Ei Electric Co., Ltd., Osaka, Japan). The kinetic process inside the cells was analyzed *via* electrochemical impedance spectroscopy (EIS) using Metrohm AUTOLAB (Utrecht, Netherlands). The amplitude of the alternating voltage was 10 mV, and the frequency range was 0.1 Hz to 10^5 Hz. The equivalent circuit

and impedance parameters were obtained by fitting the spectra with NOVA 1.10 software (Metrohm AUTOLAB, Utrecht, Netherlands).

RESULTS AND DISCUSSION

Optical Properties of the Dyes and DSSC Device

The UV-Vis and IPCE spectra are related. Both analyses demonstrate the area where the sensitizer absorbs an intense light intensity and, hence, is capable of converting the absorbed photons into electricity. The IPCE can be expressed as follows,

$$IPCE\ (\%\ ) = 1240 \times J_{ph}\ /\ \lambda \times I \tag{1}$$

or

$$IPCE\ (\lambda) = LHE \times \phi_{inj} \times \eta_{col} \tag{2}$$

where J_{ph} (mA cm^{-2}), λ (nm), and I (cm^{-2}) refer to the short circuit photocurrent density, wavelength, and intensity of the monochromatic light, respectively. ϕ_{inj} is the efficiency of electron injection from the excited dye into the TiO_2, η_{col} is the efficiency of collection of the injected electron at the electrode, and LHE is light harvest efficiency of the electrode. IPCE is indirectly related to the dye absorption observed in UV-Vis spectra (Ooyama and Harima 2012).

Figure 1 shows the absorption spectra of individual sensitizers; mengkulang and rengas dyes adsorbed onto TiO_2 thin film along with the IPCE spectra obtained from the spectral response. Mengkulang dye had a broader absorption spectrum with no intense peaks in the tested wavelengths. However, intense peaks were observed at 400 nm and 576 nm for rengas dye. Rengas dye has a lower capability to harvest light because it has a narrow absorption band (Sayama *et al*. 2003). Subsequently, the IPCE percentage of mengkulang-sensitized DSSC was higher than rengas-sensitized DSSC at the lower wavelength range (400 nm to 500 nm). However, rengas-sensitized DSSC had a good IPCE percentage at the higher range of 523 nm to 600 nm.
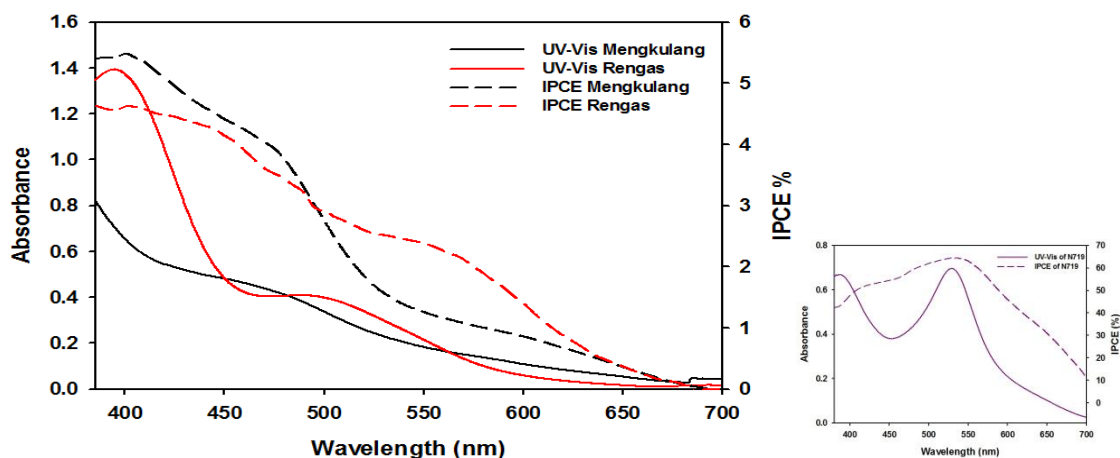

Fig. 1. UV-Vis absorption and IPCE spectra of individual mengkulang and rengas dyes. The UV-Vis and IPCE curves of ruthenium (N719)-based DSSC are shown at the side for comparison.

For mixture sensitizers, both M:R (50%:50%) and M:R (60%:40%) dyes illustrated the same pattern of absorption, as shown in Fig. 2. A broad shoulder was

observed between 500 nm and 550 nm. The M:R (60%:40%)-sensitized DSSC showed a higher IPCE, which indicated that more photons were absorbed and converted to current in the cells (Hara *et al.* 2000). The broad shoulder of IPCE spectra for mixture sensitizer was observed in the range of 550 nm to 600 nm. As compared to the absorption spectra, the shoulder was shifted to the longer wavelength. This result suggested that mixture-sensitized DSSCs had a better capability in harvesting light and converting electrons than the individual sensitized DSSCs because the absorption and IPCE spectra covered a wider range of wavelengths.
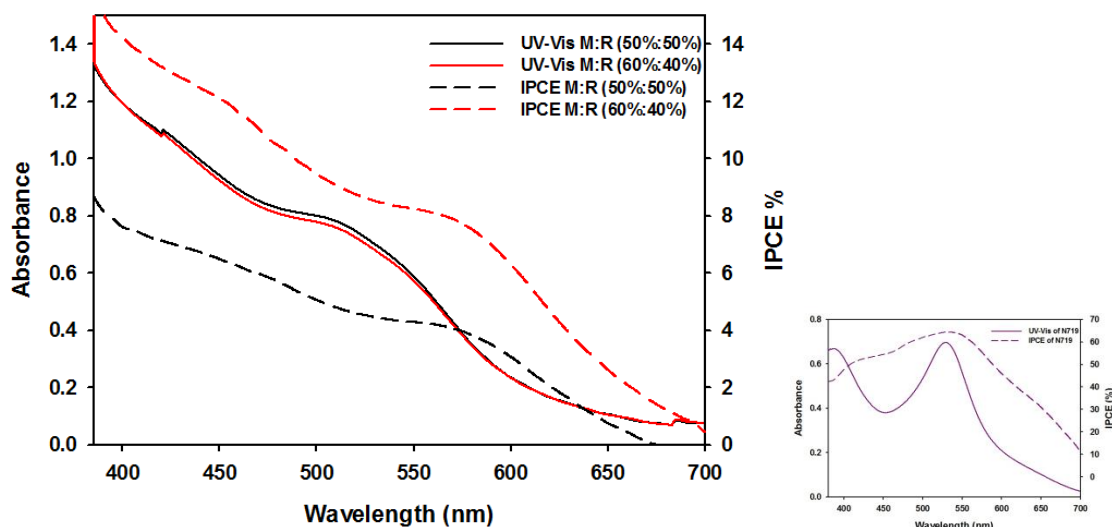

Fig. 2. UV-Vis absorption and IPCE spectra of the mixture dyes. M, mengkulang; R, rengas. The UV-Vis and IPCE curves of ruthenium (N719)-based DSSC are shown at the side for comparison.

Furthermore, for co-sensitizers, the absorption spectra had broad shoulders between 400 nm to 550 nm with no intense peak in Fig. 3. The M:N (80%:20%) and M:R:N (40%:40%:20%) sensitizers had a similar pattern. The R:N (80%:20%) sensitizer had two obvious shoulders at 420 nm and 505 nm. The absorption spectrum for co-sensitizers had broad absorption bands compared with individual and mixture sensitizers, as the ruthenium (N719) dye acted as a co-sensitizer to graft more dye molecules onto TiO_2, leading to a wider range of light absorption (Wang *et al.* 2004). The inset shows UV-Vis and IPCE curves of ruthenium (N719) dye-sensitized DSSC for comparison. The M:N (80%:20%)-sensitized DSSC had a higher IPCE percentage throughout the visible light. Both of the IPCE curves for M:N (80%:20%) and ruthenium (N719) dye-sensitized DSSCs had an intense peak at 530 nm. This result suggested that ruthenium (N719) dye enhanced the generated photocurrent *via* the addition of adsorbed dye molecules onto TiO_2 inside the M:N (80%:20%)-sensitized DSSC (Choi *et al.* 2015). In contrast, the R:N (80%:20%)-sensitized DSSC showed a lower IPCE value, suggesting that the rengas sensitizer masked the other sensitizer from efficient light harvesting and photocurrent generation. There was a similar pattern in the IPCE curves for R:N (80:20%) and M:R:N (40%:40%:20%)-sensitized DSSCs, which lacked an intense peak at 530 nm. Different sensitizers exhibit different absorption bands because of the different adsorption abilities of each sensitizer (Shahid *et al.* 2013) and eventually will lead to different patterns for the IPCE plot (Kushwaha *et al.* 2013).
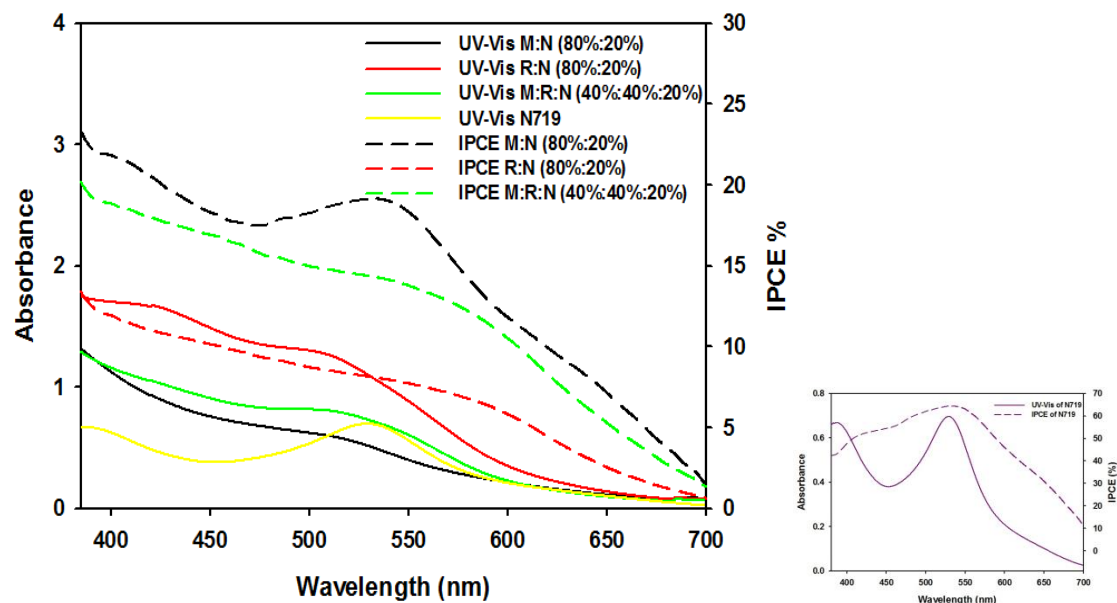
Fig. 3. UV-Vis absorption and IPCE spectra of co-sensitization dyes and their ratios. M, mengkulang; R, rengas; N, ruthenium (N719) dye. The UV-Vis and IPCE curves of ruthenium (N719)-based DSSC are shown at the side for comparison.

DSSC Device Photovoltaic Performances

Figure 4 shows the current-voltage (*I-V*) curves of individual, mixture, and co-sensitized DSSCs, and Table 1 summarizes the photovoltaic performance parameters of each DSSC. The energy conversion efficiency (η) was calculated by using Eq. 3,

$$\eta = \frac{V_{oc}\, J_{sc}\, FF}{P_{in}} \qquad (3)$$

where the open circuit voltage, V_{oc} (V) is the maximum voltage measured at the zero current condition, and the short-circuit current density, J_{sc} (mA cm^{-2}), is the maximum current density collected by the cell in short circuit condition. Both values are shown in the *I-V* curves plotted in Fig. 4. P_{in} is the intensity of the incident light (100 mW cm^{-2}), and the fill factor (FF) is defined as the ratio of optimum photocurrent and voltage with the product of V_{oc} and J_{sc}.

bioresources.com

Table 1. Current-Voltage (*I-V*) Performance and Power Conversion Efficiency (η) of DSSCs Sensitized with the Individual, Mixture, and Co-sensitized Dyes

Sensitizer	V_{oc} (V)	J_{sc} (mA cm^{-2})	ff	η (%)
Mengkulang (M)	0.53	0.40	75.98	0.16
Rengas (R)	0.50	0.30	72.88	0.11
M:R (50%:50%)	0.54	0.60	63.28	0.21
M:R (60%:40%)	0.53	0.90	62.16	0.30
M:N (80%:20%)	0.63	2.10	44.00	0.58
R:N (80%:20%)	0.53	1.10	57.07	0.33
M:R:N (40%:40%:20%)	0.55	1.60	45.23	0.39
*N719	0.82	7.40	62.55	3.80
* The ruthenium (N719)-based DSSC is shown for comparison				
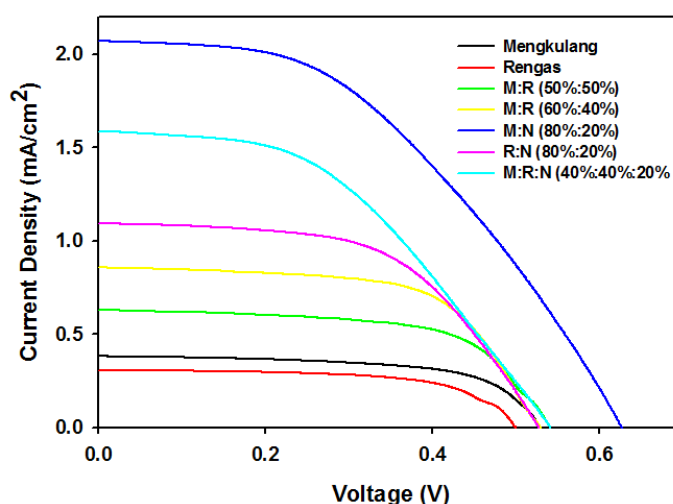
Fig. 4. I-V curves of DSSC device sensitized with individual dyes, mixture dyes, and co-sensitized dyes

For individual sensitized DSSCs, the value of open circuit voltage (V_{oc}) was almost constant (0.50 V to 0.54 V), which means that the potential difference between the electrochemical potential of electrolyte and Fermi level of semiconductor did not have much difference (Nazeeruddin *et al.* 2003). Mengkulang-sensitized DSSC achieved slightly higher conversion efficiency (η), which was 0.16% with an open circuit voltage (V_{oc}) of 0.53 V, short-circuit current density (J_{sc}) of 0.40 mA cm^{-2}, and fill factor (ff) of 75.98, compared with the results for rengas-sensitized DSSC (η: 0.11%, V_{oc}: 0.50 V, J_{sc}: 0.30 mA cm^{-2}, and ff: 72.88). Moreover, mixture-sensitized DSSCs were expected to have better performance than the individual-sensitized DSSCs due to the enhancement of absorption discussed previously. The M:R (60%:40%)-sensitized DSSC achieved better photovoltaic performance (η: 0.30%, V_{oc}: 0.53 V, J_{sc}: 0.90 mA cm^{-2}, and ff: 62.16). However, the M:R (50%:50%)-sensitized DSSC generated slightly lower photovoltaic performance (η: 0.21%, V_{oc}: 0.54 V, J_{sc}: 0.60 mA cm^{-2}, and ff: 63.28). A good increase in J_{sc} was obtained for the mixture-sensitized DSSCs, which indicated that they were capable of generating dense electron distribution at the surface of the TiO$_2$ layer and that electrons were injected effectively through the photoelectrode layer (Ooyama and Harima 2012).

The best performance among the co-sensitized DSSC was observed in the M:N (80%:20%)-sensitized DSSC, which showed the conversion efficiency (η) of 0.58% with an open circuit voltage (V_{oc}) of 0.63 V, short-circuit current density (J_{sc}) of 2.10 mA cm^{-2}, and fill factor (ff) of 44.00. The R:N (80%:20%) and M:R:N (40%:40%:20%)-sensitized DSSCs had similar conversion efficiencies (η), which were 0.33% (V_{oc}: 0.53 V, J_{sc}: 1.10 mA cm^{-2}, and ff: 57.07) and 0.39% (V_{oc}: 0.55 V, J_{sc}: 1.60 mA cm^{-2}, and ff: 45.23), respectively. Their J_{sc} and V_{oc} values were lower than the M:N (80%:20%)-sensitized DSSC. This condition suggested that the dyes did not adsorb onto the TiO$_2$ layer efficiently, which affected the electron transfer from the lowest unoccupied molecular orbital (LUMO) level to the Fermi level of TiO$_2$ (Lim *et al.* 2015). The high value of short-circuit current density ($\boldsymbol{J_{sc}}$) obtained by the M:N (80%:20%)-sensitized DSSC indicated that the high electron distribution at the surface of TiO$_2$ caused the Fermi level to shift towards the conduction band (CB) (Mora-sero and Bisquert 2003). As a result, the value of V_{oc} was higher and led to the better conversion efficiency of the cell and process. Regardless of the high photovoltaic performance shown by co-sensitized DSSCs, the presence of ruthenium (N719) dye impacted the results. Compared with the photovoltaic performance achieved by the ruthenium (N719) dye-sensitized DSSC (Table 1), the co-sensitized DSSCs showed poor performance. The kinetics of the electrochemical and the photoelectrochemical processes in the cell influenced the cell performance, as discussed in the next section.

Electrochemical Impedance Study

The electron transport parameters in the DSSC device were further analyzed by using electrochemical impedance spectroscopy (EIS). In this study, EIS analysis was carried out under one sun (AM 1.5) light intensity at an open circuit condition. The theory, parameters, and calculations of this analysis have been discussed previously (Bisquert 2002; Adachi *et al.* 2006). The impedance of the equivalent circuit indicating the diffusion-recombination effect under boundary condition is expressed as follows (Bisquert 2002; Kern *et al.* 2002; Wang *et al.* 2005),

$$Z = R_{ct} \left(\frac{1}{\left(\frac{\omega_{rec}}{\omega_d}\right)\left(1+\frac{i\omega}{\omega_{rec}}\right)} \right)^{1/2} coth \left[\left(\frac{\omega_{rec}}{\omega_d}\right)\left(1+\frac{i\omega}{\omega_{rec}}\right) \right]^{1/2} \tag{4}$$

The two important processes involved in this diffusion-recombination effect are the diffusion of an electron across the semiconductor layer of photoanode (ω_d) and the electron back reaction with oxidized redox species (ω_{rec}). These parameters can be defined as (Adachi *et al.* 2006):

$$\omega_d = D_{eff}/L^2 , \; \omega_{rec} = k_{eff} = 1/\tau_{eff} \tag{5}$$

Meanwhile, the diffusion-recombination resistances can be defined as (Adachi *et al.* 2006),

$$R_{ct} = con\frac{L}{D_{eff}} = \frac{L^2}{D_{eff}C_\mu} , \; R_{rec} = con\frac{1}{Lk_{eff}} = \frac{L_n{}^2}{D_{eff}C_\mu} \tag{6}$$

where the constant (*con*) is defined by,

$$con = \frac{K_B T}{q^2 A \eta_s} \tag{7}$$

bioresources.com

and where Z (Ω), R_{ct} (Ω), R_{rec} (Ω), ω_d (Hz), ω_{rec} (Hz), τ_{eff} (ms), $\underline{C}_\mu$, K_B (J K^{-1}), T, q, A (m^2), and η_s represent the impedance, electron transport resistance in TiO$_2$, recombination resistance, characteristic frequency correspond to the electron diffusion in TiO$_2$, characteristic frequency corresponds to the electron back reaction with oxidized redox species in the electrolyte, electron lifetime in TiO$_2$, chemical capacitance of TiO$_2$, Boltzmann constant, absolute temperature, elementary charge, area of electrode, and electron density at conduction band of TiO$_2$, respectively. The relationship between characteristic frequencies and diffusion-recombination resistances can be related as follows Eq. 8 (Bisquert 2002).

$$\frac{\omega_d}{\omega_{rec}} = \frac{R_{rec}}{R_{ct}} = \frac{L_n^2}{L^2} \tag{8}$$

From Eqs. 5 and 6, effective electron diffusion coefficient, D_{eff} (cm^2 s^{-1}) and electron diffusion length, L_n (µm) can be written as follows (Adachi *et al.* 2006; Chiu *et al.* 2009),

$$D_{eff} = \left(\frac{R_{rec}}{R_{ct}}\right) L^2 k_{eff} \tag{9}$$

$$L_n = \sqrt{\frac{D_{eff}}{k_{eff}}} = \sqrt{D_{eff}\tau_{eff}} \tag{10}$$

where the effective electron lifetime, τ_{eff} (ms) and effective recombination rate constant, k_{eff} (s^{-1}) can be expressed in the term of peak frequency, f_{max} (Hz) obtained from Bode phase plot at the range of 1 Hz to 1 kHz (Adachi *et al.* 2006; Deng *et al.* 2011).

$$\omega_{rec} = 2\pi f_{max} \tag{11}$$

Hence,

$$\tau_{eff} = \frac{1}{2\pi f_{max}} = \frac{1}{\omega_{rec}} = \frac{1}{k_{eff}} \tag{12}$$

Table 2 summarizes the electron transport properties of the DSSC device sensitized with the individual, mixture, and co-sensitized dyes. The various electron transport parameters were gained after fitting the EIS curves using NOVA 1.10 software using the equivalent circuit shown in the inset of Fig. 5. The equivalent circuit elements include sheet resistance of the conducting glass (R_s), constant phase element (CPE), and interface charge transfer resistance (R_{rec} and R_{ct}). R_{rec} is the electron transfer resistance of the charge recombination process at TiO$_2$/dye/electrolyte interface, while R_{ct} is the transport resistance of electron diffusion at TiO$_2$/dye interface. The CPE is replacing double layer capacitance, C_{dl} to account for the deviation of the C_{dl} from the ideal interfacial capacitance, which is related to the roughness of the electrode used (Omar *et al.* 2013; Sarker *et al.* 2014; Kumara *et al.* 2015).
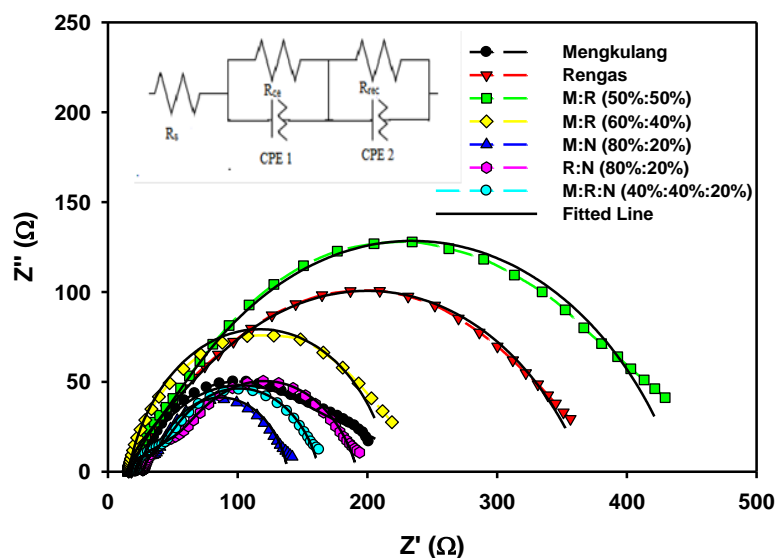
bioresources.com

Fig. 5. Nyquist plot based on the electrochemical impedance of the DSSC devices sensitized with the individual, mixture, and co-sensitized dyes. The inset shows the equivalent circuit of this study.

The Nyquist plot includes three semicircles present at different ranges of frequency. At high-frequency region between 1 kHz to 100 kHz, the arc exists due to the charge transfer at the counter electrode. In the intermediate region (1 Hz to 1 kHz), the middle arc is according to charge transfer at the TiO_2/dye/electrolyte interface meanwhile diffusion in the redox electrolyte produces an arc at low frequency (0.2 Hz to 0.75 Hz) (Omar and Abdullah 2014). However, according to literature (Sarker *et al.* 2014), DSSCs do not necessarily show three peaks in a Bode phase plot or three distinct arcs in the Nyquist plot. From the Nyquist plot in Fig. 5, the magnitude of R_{rec} at the TiO_2 layer/electrolyte interface was directly proportional to the diameter of the second arc. The device sensitized with M:R (50%:50%) had a longer diameter, followed by rengas, M:R (60%:40%), and Mengkulang, respectively. The Mengkulang-sensitized DSSC had the lowest value of R_{rec}, which was 150 Ω. The M:R (60%:40%), rengas, and M:R (50%:50%)-sensitized DSSCs had values of 202 Ω, 331 Ω, and 407 Ω, respectively.

The Nyquist plot of co-sensitized DSSC is shown in Fig. 6. The R:N (80%:20%)-sensitized DSSC had the longest diameter of the second arc and the highest value of R_{rec} (26.2 Ω). M:R:N (40%:40%:20%) and M:N (80%:20%)-sensitized DSSCs had R_{rec} values of 21 Ω and 18.3 Ω, respectively. From Table 2, the value of R_{ct} obtained was smaller than R_{rec} ($R_{rec} >> R_{ct}$) for the individual- and mixture-sensitized DSSCs. The co-sensitized DSSCs had smaller R_{rec} values than the R_{ct} ($R_{rec} << \underline{R}_{ct}$) condition. The value of R_{rec}/R_{ct} for co-sensitized DSSCs were much smaller than 1 at 0.18, 0.17, and 0.19 for M:N (80%:20%), M:R:N (40%:40%:20%), and R:N (80%:20%), respectively. The shape of the central arc deviated, especially at a higher frequency or known as Gerischer impedance (Sarker *et al.* 2013). Furthermore, only rengas and M:R (50%:50%)-sensitized DSSCs obtained an R_{rec}/R_{ct} value higher than 10, which was 17.2 and 24.1, respectively. Thus, the shape of the central arc was a true circle as shown in Fig. 5. This finding was similar to the results of Adachi *et al.* (2006).

Figures 6 and 7 show the Bode phase plot of the individual, mixture, and co-sensitized DSSCs. The parameter f_{max} within the range of 1 Hz to 1 kHz was inversely proportional to the τ_{eff} as defined in Eq. 12. f_{max} corresponds to the charge-transfer at the TiO$_2$/dye/electrolyte interface, and τ_{eff} is the time constant for how long it takes for an electron to diffuse at TiO$_2$ before the excess electron recombine. For individual and mixture-sensitized DSSCs, M:R (50%:50%)-sensitized DSSC obtained lower frequency position of f_{max} at an intermediate region of frequency followed by rengas, mengkulang, and M:R (60%:40%)-sensitized DSSCs, respectively.
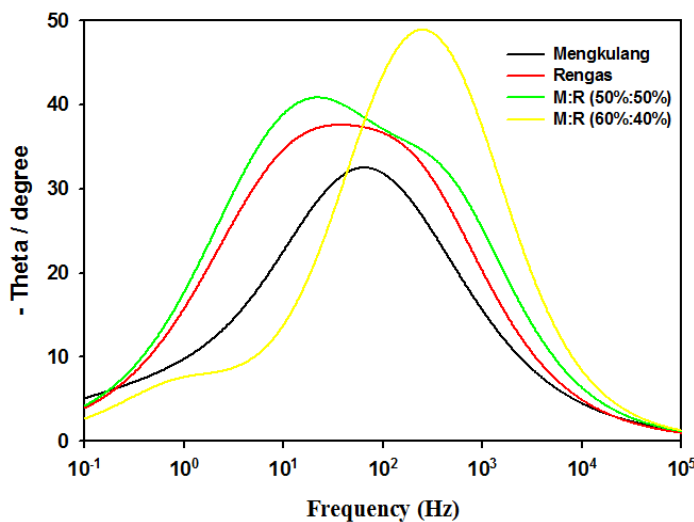

Fig. 6. Bode phase plot of DSSC devices sensitized with mengkulang, rengas, and mixtures
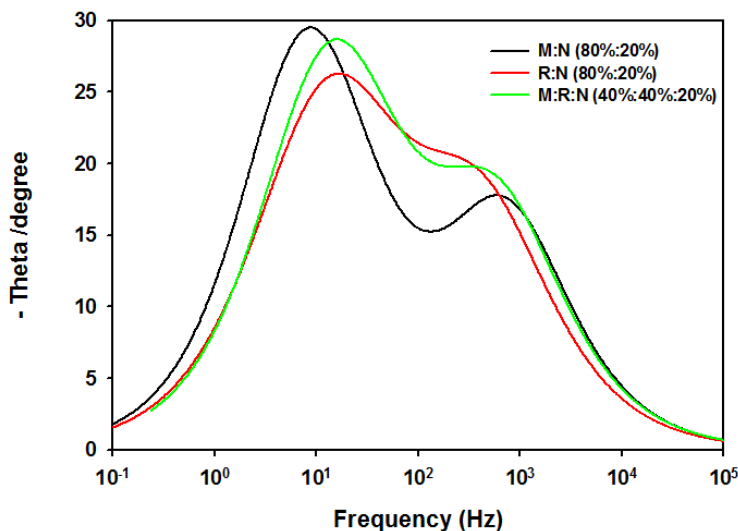

Fig. 7. Bode phase plot of the co-sensitized DSSCs

Because the f_{max} of M:R (60%:40%)-sensitized DSSC shifted to the high-frequency region, the τ_{eff} obtained was the lowest, which was 0.594 ms. Meanwhile, the M:R (50%:50%), rengas, and mengkulang-sensitized DSSCs obtained 7.508 ms, 4.272 ms, and 2.431 ms, respectively. For co-sensitized DSSCs, the position of f_{max} was at the lowest frequency of intermediate region for M:N (80%:20%)-sensitized DSSCs, thus

bioresources.com

leading to the highest value of τ_{eff}, which was 17.493 ms. However, the R:N (80%:20%) and M:R:N (80%:20%)-sensitized DSSCs obtained the same value of τ_{eff}, which was 9.953 ms because the position of f_{max} obtained was the same. This result suggests that the R:N (80%:20%) and M:R:N (80%:20%)-sensitized DSSCs achieved similar photovoltaic performance, as discussed previously.

The thickness of the TiO$_2$ thin film (*L*) measured in this study was the controlled variable (17.74 μm). The magnitude of effective electron diffusion length (L_n) was calculated using Eq. 10. L_n for mengkulang, rengas, M:R (50%:50%), and M:R (60%:40%)-sensitized DSSCs was measured to be more than *L*, with values of 31.97 μm, 73.66 μm, 87.06 μm, and 35.66 μm, respectively. This condition ($L_n \gg L$) was important for the diffusion of electrons through the photoelectrode. By referring to Eq. 7, when $L_n \gg L$ and the value of R_{rec} are finite, $R_{rec} \ll R_{ct}$, where recombination resistance must be higher than that of charge transport resistance. The higher value of R_{rec} inhibits the recombination process from occurring. This was the condition desired to achieve efficient DSSC device operation at moderate potentials (Adachi *et al.* 2006; Omar *et al.* 2013). The values of R_{rec} and R_{ct} obtained for mengkulang, rengas, M:R (50%:50%), and M:R (60%:40%)-sensitized DSSCs in this study establilshed the relationship for both conditions.

The magnitude of electron density (η_s) that accumulates at the surface of a photoelectrode could be predicted from the value of constant (*con*) calculated by using Eq. 7. A higher value of calculated *con* would lead to lower concentration of injected electrons accumulated at the conduction band of TiO$_2$. From the value of *con* in Table 2, M:R (50%:50%)-sensitized DSSC was expected to have higher electron density followed by mengkulang, rengas, and M:R (60%:40%)-sensitized DSSCs. For the co-sensitized DSSCs, the M:N (80%:20%)-sensitized DSSC was predicted to have higher electron density, followed by M : R : N (40% : 40% : 20%) and R:N (80%:20%)-sensitized DSSCs. This concentration of electrons would eventually diffuse to the photoelectrode with the effective electron diffusion coefficient (D_{eff}), as calculated by using Eq. 9 and assumed being lost with the recombination rate constant (k_{eff}), which was equal to the reciprocal of τ_{eff} (Kern *et al.* 2002). DSSC devices need a higher value of D_{eff} and η_s but a lower value of k_{eff} to achieve efficient performance (Lim *et al.* 2016). For individual and mixture-sensitized DSSCs, M:R (50%:50%)-sensitized DSSC showed the lowest value of *con* (which means higher value of η_s), and the lowest value of k_{eff} (133.2 s^{-1}) and D_{eff} were calculated to be quite low, which was 1.01×10^{-6} cm^2 s^{-1}. In contrast, the M:R (60%:40%)-sensitized DSSC was predicted to have a lower value of electron density (η_s), which means that the electrons were lost rapidly. This was demonstrated by a shorter electron lifetime (τ_{eff}) and the higher rate of recombination (k_{eff}), which was 1684.7 s^{-1}. However, D_{eff} was recorded as 2.14×10^{-6} cm^2 s^{-1}, which was much larger than that of the M:R (50%:50%)-sensitized DSSC. Thus, faster electron transport through TiO$_2$ layer was expected where it eventually increased the photocurrent density at the photoelectrode. This explained why the value of J_{sc} achieved for M:R (60%:40%)-sensitized DSSC was higher than M:R (50%:50%)-sensitized DSSC, thus leading to higher conversion efficiency (η).

Table 2. Electron Transport Properties of the DSSC Device Sensitized with Individual, Mixture, and Co-Sensitized Dyes Determined by Electrochemical Impedance Spectroscopy

Sensitizer	R_{rec} (Ω)	R_{ct} (Ω)	D_{eff} (cm^2 s^{-1})	k_{eff} (s^{-1})	τ_{eff} (ms)	L_n (μm)	Con (Ω cm s^{-1})
Mengkulang (M)	150.0	46.2	4.20×10^{-7}	411.4	2.431	31.97	1.090
Rengas (R)	331.0	19.2	1.27×10^{-6}	234.1	4.272	73.66	1.370
M:R (50%:50%)	407.0	16.9	1.01×10^{-6}	133.2	7.508	87.06	0.962
M:R (60%:40%)	202.0	50.0	2.14×10^{-6}	1684.7	0.594	35.66	6.040
M:N (80%:20%)	18.3	103.0	3.20×10^{-9}	57.2	17.493	7.48	0.019
R:N (80%:20%)	26.2	139.0	5.96×10^{-9}	100.5	9.953	7.70	0.047
M:R:N (40%:40%:20%)	21.0	121.0	5.49×10^{-9}	100.5	9.953	7.39	0.037

Moreover, for the co-sensitized DSSCs, the M:N (80%:20%)-sensitized DSSC achieved the lowest value of *con* (which means higher η_s), and lowest k_{eff} (57.2 s^{-1}) as compared to R:N (80%:20%)- and M:R:N (80%:20%)-sensitized DSSCs, which both obtained the same value of k_{eff} (100.5 s^{-1}). There was a big difference in the D_{eff} values calculated for the M:N (80%:20%)-sensitized DSSC. The conversion efficiency (η) was the highest value because the effective electron lifetime (τ_{eff}) of M:N (80%:20%) sensitized DSSC is the longest. Hence, the distribution of electrons at the porous semiconductor had enough time to diffuse across the TiO$_2$ layer before recombination took place. Even though the conversion efficiency of co-sensitized DSSCs was higher than that of individual and mixture-sensitized DSSCs, they were much lower than the ruthenium (N719) dye-sensitized DSSC (Table 1). The R_{ct} value was higher than that of R_{rec} ($R_{rec} \ll R_{ct}$) for all co-sensitized DSSCs. In this case, the recombination time was much faster than that of electron diffusion. By referring to the results in Table 2, the value obtained for L_n was also lower than the value of L ($L_n \ll L$). This was the condition in where the distribution electrons being lost faster and undergo recombination before they could be injected to the conduction band and diffuse across the TiO$_2$ layer. In sum, the conditions of ($R_{rec} \ll R_{ct}$) and ($L_n \ll L$) were considered irrelevant and should be avoided in order to achieve the efficient performance of DSSC devices.

CONCLUSIONS

1. DSSCs were fabricated with natural sensitizers extracted from rengas (*Gluta* spp.) and mengkulang (*Heritiera elata*) wood. Different types of sensitizers were introduced, including individual, mixture, and co-sensitized sensitizer. The photovoltaic performance of mixture sensitized DSSCs up to 2-fold increased short-circuit current density (J_{sc}) compared with individual sensitized DSSCs, indicating improved conversion efficiency.

2. From the IPCE curve, a higher photocurrent was achieved for the M:R (60%:40%)-sensitized DSSC, which revealed good light harvesting, charge collection, and dye regeneration efficiency.

3. Electron transport behavior in the cells was estimated from the electrochemical impedance spectroscopy analysis. Even though M:R (50%:50%) obtained lower recombination rate, k_{eff}, and high estimated electron density, η_s, the conversion

bioresources.com

efficiency was slightly lower than that of the M:R (60%:40%)-sensitized DSSC because of the electron diffusion coefficient, D_{eff}, was lower.

4. Other parameters that were important to the suitability of the sensitizer occurred when $R_{\text{rec}} \gg R_{\text{ct}}$ and $L_n \gg L$ conditions were achieved. In this study, both individual and mixture-sensitized DSSCs followed these conditions. However, co-sensitized DSSCs created the phenomenon in which $R_{\text{rec}} \ll R_{\text{ct}}$ and $L_n \ll L$. In this case, the boundary condition was considered irrelevant and should have been avoided.

5. An efficient sensitizer needs a high electron diffusion coefficient, D_{eff}, low recombination rate, k_{eff}, and high electron density, η_s. The conversion efficiency achieved for M:N (80%:20%), R:N (80%: 0%), and M:R:N (80%:20%)-sensitized DSSCs was higher than individual and mixture-sensitized DSSCs; they were considered not suitable as sensitizers.

6. These findings suggested that the mixture sensitizers have great potential to improve the electrical properties and efficiency of sensitizers.

ACKNOWLEDGMENTS

REFERENCES CITED

Adachi, M., Sakamoto, M., Jiu, J., Ogata, Y., and Isoda, S. (2006). "Determination of parameters of electron transport in dye-sensitized solar cells using electrochemical impedance spectroscopy," *The Journal of Physical Chemistry B* 110(28), 13872-13880. DOI: 10.1021/jp061693u

Adeloye, A. O., and Ajibade, P. A. (2014). "Towards the development of functionalized polypyridine ligands for Ru(II) complexes as photosensitizers in dye-sensitized solar cells (DSSCs)," *Molecules* 19(8), 12421-12460. DOI: 10.3390/molecules190812421

Basheer, B., Mathew, D., George, B. K., and Nair, C. P. R. (2014). "An overview on the spectrum of sensitizers: The heart of dye sensitized solar cells," *Solar Energy* 108, 479-507. DOI: 10.1016/j.solener.2014.08.00

Bisquert, J. (2002). "Theory of the impedance of electron diffusion and recombinantion in a thin layer," *Journal of Physical Chemistry B* 106, 325-333. DOI: 10.1021/jp011941g

Chiu, W.-H., Lee, C.-H., Cheng, H.-M., Lin, H.-F., Liao, S.-C., Wu, J.-M., Hsieh, W.-F. (2009). "Efficient electron transport in tetrapod-like ZnO metal-free dye-sensitized solar cells," *Energy & Environmental Science* 2(6): 694. DOI:10.1039/b902595m

Choi, H., Hwang, T., Lee, S., Nam, S., Kang, J., Lee, B., and Park, B. (2015). "The construction of tandem dye-sensitized solar cells from chemically derived nanoporous photoelectrodes," *Journal of Power Sources* 274, 937-942. DOI: 10.1016/j.jpowsour.2014.10.125

Deng, J., Zheng, Y. Z., Hou, Q., Chen, J. F., Zhou, W., and Tao, X. (2011). "Solid-state

dye-sensitized hierarchically structured ZnO solar cells," *Electrochimica Acta* 56(11), 4176–4180. DOI:10.1016/j.electacta.2011.01.099

Faccio, R., Fernández-Werner, L., Pardo, H., and Mombré, A. W. (2011). "Current trends in materials for dye sensitized solar cells," *Recent Patents on Nanotechnology* 5(1), 46i61. DOI:10.2174/187221011794474930

Hara, K., Horiguchi, T., Kinoshita, T., Sayama, K., Sugihara, H., and Arakawa, H. (2000). "Highly efficient photon-to-electron conversion of mercurochrome-sensitized nanoporous ZnO solar cells," *Chemistry Letters* 29(4), 316-317. DOI: 10.1246/cl.2000.316

Hara, K., Sato, T., Katoh, R., Furube, A., Yoshihara, T., Murai, M., Kurashige, M., Ito, S., Shinpo, A., Suga. S. (2005). "Novel conjugated organic dyes for efficient dye-sensitized solar cells," *Advanced Functional Materials* 15(2), 246-252. DOI: 10.1002/adfm.200400272

Kartini, I., Dwitasari, L., Wahyuningsih, T. D., and Wang, L. (2015). "The sensitization of xanthophylls-chlorophyllin mixtures on titania solar cells," *International Journal of Science and Engineering (IJSE)* 109-114.

Kern, R., Sastrawan, R., Ferber, J., Stangl, R., and Luther, J. (2002). "Modeling and interpretation of electrical impedance spectra of dye solar cells operated under open-circuit conditions," *Electrochimica Acta* 47(26), 4213-4225. DOI: 10.1016/S0013-4686(02)00444-9

Koyama, Y., Miki, T., Wang, X. F., and Nagae, H. (2009). "Dye-sensitized solar cells based on the principles and materials of photosynthesis: Mechanisms of suppression and enhancement of photocurrent and conversion efficiency," *International Journal of Molecular Sciences* 10(11), 4575-4622. DOI: 10.3390/ijms10114575

Kumara, N. T. R. N., Petrovic, M., Peiris, D. S. U., Marie, Y. A., Vijila, C., Petra, M. I., Chandrakanthi, R. L. N., Lim, C. M., Hobley, J., Ekanayake, P. (2015). "Efficiency enhancement of Ixora floral dye sensitized solar cell by diminishing the pigments interactions," *Solar Energy* 117, 36-45. DOI:10.1016/j.solener.2015.04.019

Kushwaha, R., Srivastava, P., and Bahadur, L. (2013). "Natural pigments from plants used as sensitizers for TiO_2 based dye-sensitized solar cells," *Journal of Energy* 2013, article no. 654953, 8 pp. DOI: 10.1155/2013/654953

Lim, A., Ekanayake, P., Lim, L. B. L., and Bandara, J. M. R. S. (2016). "Co-dominant effect of selected natural dye sensitizers in DSSC performance," *Spectrochimica Acta - Part A: Molecular and Biomolecular Spectroscopy* 167, 26-31. DOI: 10.1016/j.saa.2016.05.024

Lim, A., Haji Manaf, N., Tennakoon, K., Chandrakanthi, R. L. N., Lim, L. B. L., Bandara, J. M. R. S., and Ekanayake, P. (2015). "Higher performance of DSSC with dyes from cladophora sp. as mixed co sensitizer through synergistic effect," *Journal of Biophysics* 2015, Article ID 510467. DOI: 10.1155/2015/510467

Marwa, B. M., Bruno, S., Mongi, B., Tran Van, F., and Abdelmottaleb, B. L. (2016). "Modeling of adsorption isotherms of dye N719 on titanium oxide using the grand canonical ensemble in statistical physics for dye sensitized solar cells," *Solar Energy* 135, 177-187. DOI: 10.1016/j.solener.2016.05.015

Mathew, S., Yella, A., Gao, P., Humphry-Baker, R., Curchod, B. F. E., Ashari-Astani, N., Tavernelli, I., Rothlisberger, U., Nazeeruddin, M. K., and Grätzel, M. (2014). "Dye-sensitized solar cells with 13% efficiency achieved through the molecular engineering of porphyrin sensitizers," *Nature Chemistry* 6(3), 242-247. DOI: 10.1038/nchem.1861

bioresources.com

Mora-sero, I., and Bisquert, J. (2003). "Fermi level of surface states in TiO$_2$ nanoparticles," *Nano Letters* 3(7), 945-949. DOI: 10.1021/nl0342390

Narayan, M. R. (2012). "Review: Dye sensitized solar cells based on natural photosensitizers," *Renewable and Sustainable Energy Reviews* 16(1), 208-215. DOI:10.1016/j.rser.2011.07.148

Nazeeruddin, M. K., Pèchy, P., Renouard, T., Zakeeruddin, S. M., Humphry-Baker, R., Cointe, P., Liska, P., Cevey, L., Costa, E., Shklover, V. (2001). "Engineering of efficient panchromatic sensitizers for nanocrystalline TiO$_2$-based solar cells," *Journal of the American Chemical Society* 123(c), 1613-1624. DOI: 10.1021/ja003299u

Nazeeruddin, M. K., Splivallo, R., Liska, P., Comte, P., and Grätzel, M. (2003). "A swift dye uptake procedure for dye sensitized solar cells," *Chemical Communications (Cambridge, England)* 1456-1457. DOI: 10.1039/b302566g

Olea, A., Ponce, G., and Sebastian, P. J. (1999). "Electron transfer via organic dyes for solar conversion," *Solar Energy Materials and Solar Cells* 59(1), 137-143. DOI:10.1016/S0927-0248(99)00038-0

Omar, A., and Abdullah, H. (2014). "Electron transport analysis in zinc oxide-based dye-sensitized solar cells: A review," *Renewable and Sustainable Energy Reviews* 31(March): 149-157. DOI:10.1016/j.rser.2013.11.031

Omar, A., Abdullah, H., Yarmo, M. A, Shaari, S., and Taha, M. R. (2013). "Morphological and electron transport studies in ZnO dye-sensitized solar cells incorporating multi- and single-walled carbon nanotubes," *Journal of Physics D-Applied Physics* 46, 8. DOI: 10.1088/0022-3727/46/16/165503

Ooyama, Y., and Harima, Y. (2012). "Photophysical and electrochemical properties, and molecular structures of organic dyes for dye-sensitized solar cells," *Chem. Phys. Chem.* 13(18), 4032-4080. DOI: 10.1002/cphc.201200218

Ozuomba, J. O., Okoli, L. U., Ekpunobi, A. J., and Science, F. (2013). "The performance and stability of anthocyanin local dye as a photosensitizer for DSSCs," *Advances in Applied Science Research* 4(2), 60-69.

Safie, N. E., Ludin, N. A., Hisham, N., Sepeai, S., Mat Teridi, M. A., Ibrahim, M. A., Sopian, K., and Arakawa, H. (2017). "Energy levels of natural sensitizers extracted from rengas (*Gluta* spp.) and mengkulang (*Heritiera elata*) wood for dye-sensitized solar cells," *Materials for Renewable and Sustainable Energy* 6(5). DOI: 10.1007/s40243-017-0089-1

Sarker, S., Seo, H. W., and Kim, D. M. (2013). "Electrochemical impedance spectroscopy of dye-sensitized solar cells with thermally degraded N719 loaded TiO$_2$," *Chemical Physics Letters* 585, 193-197. DOI: 10.1016/j.cplett.2013.08.101

Sarker, S., Ahammad, A. J. S., Seo, H. W., and Kim, D. M. (2014). "Electrochemical impedance spectra of dye-sensitized solar cells: Fundamentals and spreadsheet calculation," *International Journal of Photoenergy* 2014. DOI:10.1155/2014/851705

Sayama, K., Tsukagoshi, S., Mori, T., Hara, K., Ohga, Y., Shinpou, A., Abe, Y., Suga, S., and Arakawa, H. (2003). "Efficient sensitization of nanocrystalline TiO$_2$ films with cyanine and merocyanine organic dyes," *Solar Energy Materials and Solar Cells* 80(1), 47-71. DOI: 10.1016/S0927-0248(03)00113-2

Shahid, M., Shahid, U. I., and Mohammad, F. (2013). "Recent advancements in natural dye applications: A review," *Journal of Cleaner Production* 53, 310-331. DOI: 10.1016/j.jclepro.2013.03.031

Shalini, S., Prabhu, R. B., Prasanna, S., Tapas, K. M., and Senthilarasu, S. (2015). "Review on natural dye sensitized solar cells: Operation, materials and methods,"

bioresources.com

Renewable and Sustainable Energy Reviews 1306-1325. DOI: 10.1016/jser.2015.07.052

Shanmugam, V., Manoharan, S., Anandan, S., and Murugan, R. (2013). "Performance of dye-sensitized solar cells fabricated with extracts from fruits of ivy gourd and flowers of red frangipani as sensitizer," *Spectrochimica Acta - Part A: Molecular and Biomolecular Spectroscopy* 104, 35-40. DOI: 10.1016/j.saa.2012.11.098

Wang, Q., Wang, Q., Moser, J.-E., Moser, J.-E., and Grätzel, M. (2005). "Electrochemical impedance spectroscopic analysis of dye-sensitized solar cells,". *The Journal of Physical Chemistry. B* 109, 14945-14953. DOI:10.1021/jp052768h

Wang, X., Kitao, O., Hosono, E., Zhou, H., Sasaki, S., and Tamiaki, H. (2010). "TiO_2 - and ZnO-based solar cells using a chlorophyll a derivative sensitizer for light-harvesting and energy conversion," *Journal of Photochemistry & Photobiology, A: Chemistry* 210(2–3), 145-152. DOI: 10.1016/j.jphotochem.2010.01.004

Wang, Z. S., Kawauchi, H., Kashima, T., and Arakawa, H. (2004). "Significant influence of $TiO2$ photoelectrode morphology on the energy conversion efficiency of N719 dye-sensitized solar cell," *Coordination Chemistry Reviews* 248(13–14), 1381-1389. DOI: 10.1016/j.ccr.2004.03.006

Wang, Z., Ju, M. G., and Liang, W. Z. (2016). "Electronic excitation and injection of Ru-N3 dye anchored to TiO_2 surface," *Computational and Theoretical Chemistry* 1097, 8-14. DOI: 10.1016/j.comptc.2016.10.006

Zeng, Z., Zhang, B., Li, C., Peng, X., Liu, X., Meng, S., and Feng, Y. (2014). "A key point of porphyrin structure affect DSSCs performance based on porphyrin sensitizers," *Dyes and Pigments* 100(1), 278-285. DOI: 10.1016/j.dyepig.2013.07.037